Wind and Structures, Vol. 9, No. 3 (2006) 193-215
DOI: http://dx.doi.org/10.12989/was.2006.9.3.193

An investigation of the wind statistics and extreme gust events at a rural site

M. Sterling[†] and C. J. Baker[‡]

School of Engineering, The University of Birmingham, Edgbaston, Birmingham, B15 2TT, UK

P. J. Richards[‡†]

School of Engineering, University of Auckland, New Zealand

R. P. Hoxey[‡‡] and A. D. Quinn[‡‡†]

School of Engineering, The University of Birmingham, Edgbaston, Birmingham, B15 2TT, UK
(Received August 1, 2005, Accepted March 15, 2006)

Abstract. This paper presents an analysis of wind velocity measurements obtained from four ultrasonic anemometers arranged in a vertical formation. The anemometers were located in a rural environment with a view to providing detailed information on the flow statistics of the lower part of the atmospheric boundary layer, particularly for the extreme wind events that are important in loading calculations. The data is analysed using both conventional analysis and conditional sampling. The latter is combined with wavelet analysis in order to provide a detailed analysis of the energy/frequency relationship of the extreme events. The work presented in this paper suggests that on average the extreme events occur as a result of the superposition of two independent mechanisms - large scale events that scale on the atmospheric boundary layer thickness and small scale events a few tens of metres in size.

Keywords: turbulence; coherent structures.

1. Introduction

The nature of the flow structures that can exist within a boundary layer is highly complex in terms of the actual physical behaviour they exhibit and also in terms of their definitions. For example, numerous references to horseshoe vorticies, hairpin eddies, pancake eddies, surfboard eddies, vortex rings and mushroom eddies can be found in the literature (Fiedler 1988). This range

† Lecturer, Corresponding Author, E-mail: m.sterling@bham.ac.uk
‡ Professor
‡† Associate Professor
‡‡ Honorary Professor
‡‡† Roberts Research Fellow

of definitions and terminology poses a number of problems since, if the scientific community cannot agree on what phenomena exists in the boundary layer, how can they ensure that they are correctly reproduced in either wind tunnel or CFD simulations? Sterling, *et al.* (2005) recently demonstrated the difficulties associated with trying to identify vortex structures within the flow even when given detailed simultaneous measurements of both velocity and static pressure. In addition, Sterling, *et al.* (2003) and Baker (2001) have shown the importance of discrete flow structures in terms of structural loading on a portal frame structure and a free standing wall respectively. Both these structures were situated in a rural location with a large uninterrupted upstream fetch, i.e., no other surrounding buildings or terrain features influenced the flow and as such the physics of the atmospheric boundary layer (ABL) should have been relatively simple to explain, when compared to, for example, the same structures but within an urban environment.

In this paper a detailed analysis of the flow statistics obtained from four ultrasonic anemometers placed in a rural location is undertaken with a view to examining the extreme statistics and hence to obtain an insight into the flow structures. Section 2 of the paper outlines the full scale experimental data in terms of standard statistical parameters (means, variances, etc.) and velocity spectra. Previous work by Baker (2001) and Sterling, *et al.* (2003, 2005) have illustrated that a significant amount of information regarding the correlation of extreme events with particular time period or length scales can be obtained by conditional sampling. This analysis is performed in Section 3 of this paper with particular reference to the instantaneous distribution of kinetic energy with respect to time. Conditional sampling and wavelet analysis are combined in order to provide an insight into the flow features of lower part of the ABL. Section 4 then discusses the results that have been obtained and the implications for loading studies. Conclusions are then drawn and presented in Section 5.

2. Experimental data

2.1. Standard statistics

The experimental velocity measurements analysed in this paper were recorded in natural wind conditions at the wind engineering site at the former Silsoe Research Institute, Bedford, UK. The experimental site is well documented (Richards, *et al.* 1997) and is orientated to face the prevailing WSW winds with a large unobstructed fetch. Four three component ultrasonic anemometers (R3 Research, Gill Instruments, Lymington, UK) were positioned at heights 1 m, 3 m, 6 m and 10 m above the ground and sampled simultaneously at a rate of 0.1s. The data presented in this paper represents 12 hours worth of continuous data, which for the purpose of the analysis has been divided into 12 separate one hour files numbered ds1 – ds12. Table 1 gives the standard flow statistics for each of the datasets. The first four columns in Table 1 are the mean streamwise velocity U for each of the ultrasonic anemometers. The headings of these columns (1, 3, 6 and 10) refer to the location of the anemometers, i.e., 1 m above the ground, 3 m above the ground etc. The fifth and sixth columns give the friction velocity u_* and surface roughness length z_0, both of which have been obtained by fitting a logarithmic velocity profile to the experimental data. The next twelve columns give the values of the turbulence intensities I_u, I_v, I_w (standard deviation/mean) of the three velocity components u, v and w. The final three columns illustrate the calculated longitudinal length scales which were obtained by integrating the autocorrelation coefficient with respect to time lag and assuming that Taylor's frozen turbulence hypothesis is valid. The final three

Table 1 Standard statistical analysis parameters

	U (m/s)				u_* (m/s)	z_0 (m)	I_u				I_v				I_w				${}^xL_u$ (m)			
Height (m)	1	3	6	10			1	3	6	10	1	3	6	10	1	3	6	10	1	3	6	10
ds1	7.29	9.01	9.91	10.54	0.57	0.0056	0.24	0.20	0.19	0.18	0.20	0.17	0.15	0.15	0.08	0.07	0.07	0.08	73	116	172	194
ds2	6.93	8.61	9.46	10.06	0.54	0.0058	0.24	0.20	0.19	0.18	0.19	0.16	0.15	0.15	0.08	0.07	0.08	0.08	73	118	157	183
ds3	6.88	8.56	9.42	10.00	0.55	0.0061	0.23	0.19	0.18	0.17	0.19	0.16	0.14	0.14	0.08	0.07	0.07	0.08	55	95	115	121
ds4	6.75	8.39	9.20	9.78	0.53	0.0056	0.23	0.20	0.19	0.18	0.20	0.17	0.15	0.15	0.08	0.07	0.08	0.08	83	140	171	190
ds5	7.21	8.92	9.87	10.46	0.56	0.0058	0.24	0.21	0.19	0.19	0.20	0.17	0.15	0.16	0.08	0.07	0.08	0.08	54	88	113	122
ds6	7.12	8.85	9.77	10.37	0.57	0.0064	0.24	0.21	0.19	0.19	0.19	0.16	0.14	0.15	0.08	0.07	0.08	0.08	90	148	190	207
ds7	7.03	8.68	9.51	10.11	0.54	0.0050	0.24	0.20	0.18	0.18	0.19	0.16	0.14	0.14	0.08	0.07	0.08	0.08	84	139	186	208
ds8	6.86	8.50	9.36	10.00	0.55	0.0063	0.25	0.22	0.20	0.20	0.20	0.17	0.15	0.15	0.08	0.07	0.08	0.09	82	136	175	204
ds9	6.36	7.92	8.71	9.25	0.50	0.0061	0.25	0.21	0.20	0.19	0.20	0.17	0.15	0.16	0.08	0.08	0.08	0.09	69	107	135	151
ds10	7.16	8.87	9.77	10.43	0.57	0.0063	0.25	0.21	0.20	0.19	0.20	0.17	0.15	0.15	0.08	0.08	0.08	0.09	88	141	178	205
ds11	6.97	8.70	9.62	10.25	0.57	0.0073	0.26	0.22	0.21	0.20	0.21	0.18	0.16	0.16	0.08	0.07	0.08	0.08	69	118	150	184
ds12	7.09	8.79	9.68	10.30	0.56	0.0061	0.25	0.22	0.20	0.19	0.21	0.17	0.15	0.15	0.08	0.07	0.08	0.09	96	133	176	201
Average =	6.97	8.65	9.52	10.13	0.55	0.0060	0.24	0.21	0.19	0.19	0.20	0.17	0.15	0.15	0.08	0.072	0.078	0.083	76	122	160	180
Stdev =	0.25	0.29	0.33	0.36	0.02	0.0005	0.01	0.01	0.01	0.01	0.01	0.01	0.01	0.01	0.02	0.02	0.02	0.02	13	19	26	32
CoV (%) =	3.6	3.4	3.5	3.5	3.8	8.9	3.6	4.7	4.6	4.8	3.6	3.7	3.9	4.4	0.0	5.4	5.0	5.9	17	16	16	17

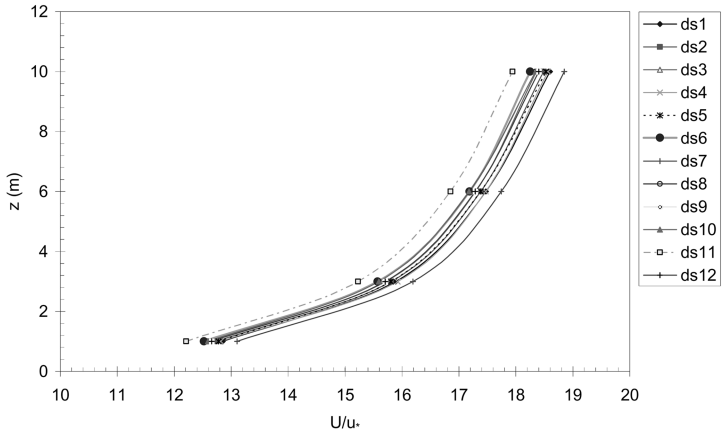

Fig. 1 Variation of normalised streamwise velocity with height

rows in Table 1 give the average, standard deviation and coefficient of variation (100 × standard deviation/mean) of all of the values in each of the corresponding columns.

The most striking feature of Table 1 is the similarity between all of the twelve datasets. For example, there is little variation in hourly mean velocity between consecutive hours and over the whole period of the test. The overall coefficient of variation (CoV) of mean velocity does not exceed 3.6% for any of the anemometers. The increase in mean velocity with respective to height is apparent (Fig. 1) and has enabled sensible values of u_* and z_0 to be determined from a logarithmic plot. Despite the errors that can occur with this process there is little variation in both of these parameters (3.8% and 8.9% for u_* and z_0 respectively). The longitudinal turbulence intensity values show a decrease with height (Fig. 2a), are reasonably consistent across all of the datasets (maximum CoV ~5%) and are appropriate for this type of rural terrain (ESDU 1985). The lateral turbulence intensities shown in Fig. 2(b) illustrate similar results to that of Fig. 2(a), namely that all of the data pertaining to this parameter exhibits little variation between each dataset (maximum CoV ~5%) and there is a general decrease in I_v with increasing height. The ratio of σ_v/σ_u across all of the datasets is within a narrow range and takes an average value of 0.8. This is consistent with previously published data corresponding to similar terrain (ESDU 1985).

The vertical turbulence shown in Fig. 2(c) and the corresponding data in Table 1 highlights that this parameter is reasonably consistent across all of the datasets and that there is little variation with height. σ_w/σ_u across all of the datasets varies with height and attains an average value of 0.45 at 10m. This is somewhat lower than the 0.52 value quoted in ESDU (1985), but it is felt that this is still within acceptable limits. The length scales in Table 1 are less consistent than the rest of the data. These inconsistencies are not unexpected given the errors which are prone to occur in such calculations. For example, Sterling, *et al.* (2005) illustrate that using different methods to calculate the length scales can result in variations of up to 300%. Nevertheless on the whole the data show an increase with height.

In order to establish the stability of the flow the ratio of height to Monin-Obukhov length (z/L_{mo}) was calculated using (Kaimal and Finnigan 1994):

$$\frac{z}{L_{mo}} = \frac{(-g/\theta)(\overline{w'\theta'})_0}{u_*^3/\kappa z} \tag{1}$$

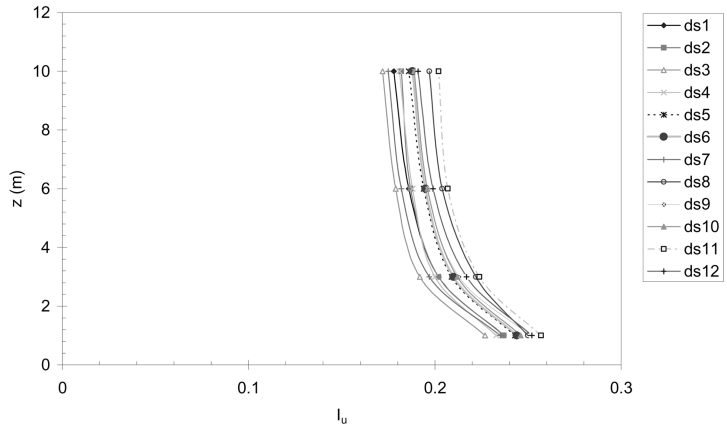

(a) Longitudinal turbulence intensity

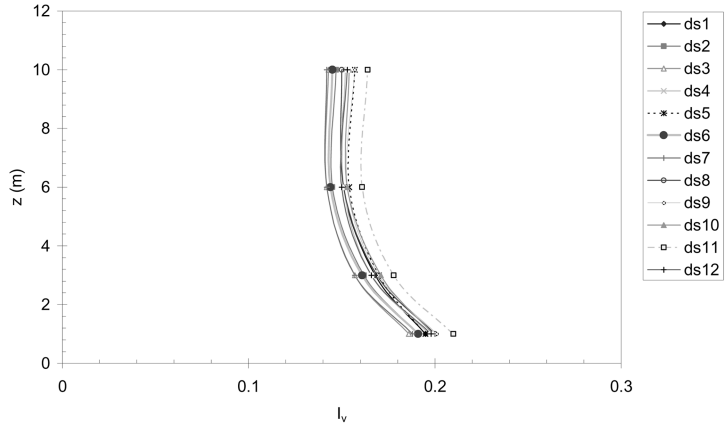

(b) Lateral turbulence intensity

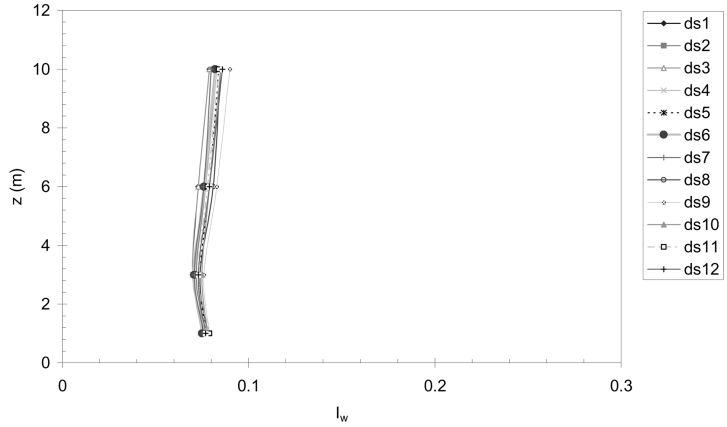

(c) Vertical turbulence intensity

Fig. 2 Variation of turbulence intensity with height

where g is the acceleration due to gravity, θ is the mean potential temperature, κ is the von-Karman constant and $\overline{(w'\theta')}_0$ was evaluated from the measurements at $z = 1$ m. The values of z/L_{mo} for all of the datasets at the four heights above the ground were ranged from 0.001 to 0.04 indicating that in

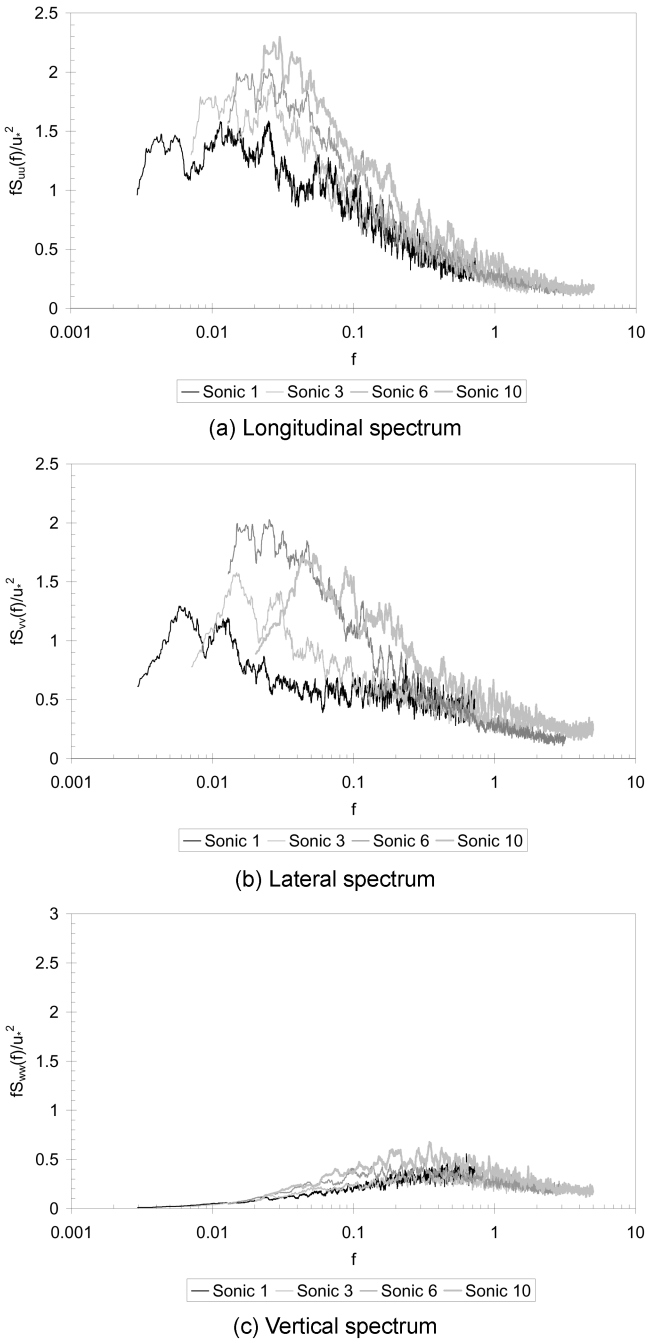

Fig. 3 Velocity spectra for ds3

all cases the flow can be considered as neutral (Stull 1988).

Although these standard statistics are useful in quantifying a number of flow features and enabling initial, broad comparisons between the datasets to be made, they yield little information in terms of understanding the physics of the flow, beyond that which is already known. However, the information contained in Table 1 is sufficient to ensure that the datasets are superficially similar to enable direct comparison. In order to extract further information from the data regarding possible

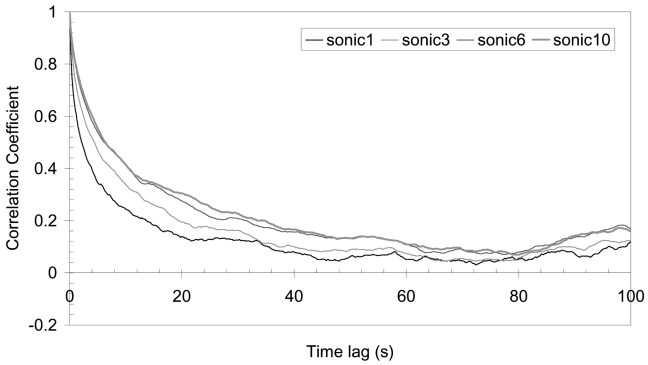

(a) Longitudinal velocity

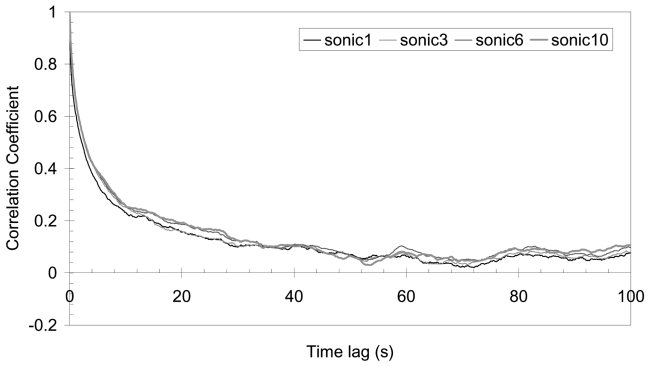

(b) Lateral velocity

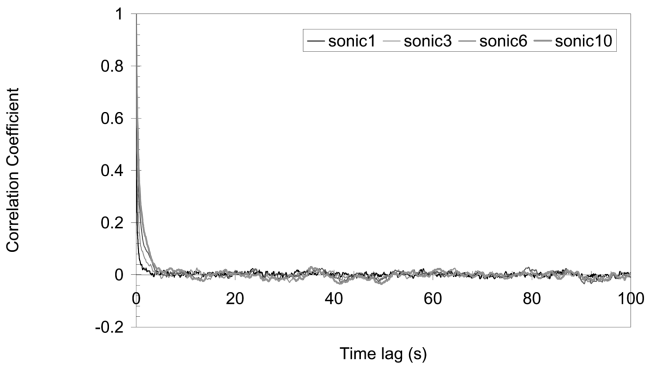

(c) Vertical velocity

Fig. 4 Velocity component autocorrelations for ds1

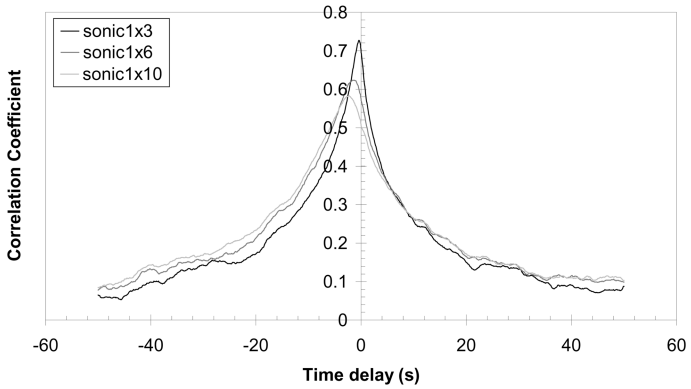

Fig. 5 Cross correlation data for ds1

flow structures attention will now be focused on examining the spectral and turbulent kinetic energy characteristics of the flow.

2.2. Velocity spectra and correlations

Similar data obtained in the same environment has been thoroughly analysed in the spectral domain by Richards, *et al.* (1997) and such an analysis is presented in this paper only to demonstrate that the data has the appropriate spectral characteristics. The streamwise, lateral and vertical velocity spectra are shown in Fig. 3 for a single test, ds3, with the other datasets illustrating similar characteristics. In order to aid comparison the spectra have been plotted in terms of reduced frequency f which is equivalent to nz/U where n is the actual frequency. The spectra clearly illustrate two distinct regions: one region corresponding to low frequency scales and the second region relating to the high frequency range.

The length scales obtained in Table 1 were calculated by integrating the autocorrelation function. Fig. 4 shows a typical distribution of autocorrelation function of the velocity data with respect to the time lag (ds1). Fig. 4 and similar figures corresponding to other datasets (not shown here) illustrate that a rapid decrease in correlation with values of time lag of a few seconds. Fig. 5 illustrates the cross correlation of the streamwise velocity component at a height of 1 m above the ground with the streamwise velocity component at heights of 3 m, 6 m and 10 m. As would be expected, as the distance from the ultrasonic anemometer at 1 m above the ground increases the maximum value of cross correlation reduces. Table 2 shows the maximum values of cross correlation for all tests and the time lags at which these maximum values occur. In Table 2 the first column refers to the specific data set, while the following three columns (1×3, 1×6, and 1×10) give the maximum value of the cross correlation of anemometer one with anemometer three, anemometer one with anemometer six and anemometer one with anemometer ten respectively. Table 2 illustrates that there is little variation in this parameter with the maximum value of the coefficient of variation (CoV) equal to 3.8%. As the vertical distance between the anemometers increases the average value of correlation reduces and the CoV increases to 3.8%. It is interesting to note that the average time lag also increases between the events, indicating that the structure passes first through the 10 m ultrasonic anemometer anemometer, the 6 m ultrasonic anemometer anemometer, and the 3 m ultrasonic anemometer before it is detected by the ultrasonic anemometer at 1 m.

Table 2 Maximum cross correlation values and corresponding time delays for the streamwise velocity component

	1×3		1×6		1×10	
	Max correlation	Time (s)	Max correlation	Time (s)	Max correlation	Time (s)
ds1	0.727	-0.4	0.623	-1.7	0.583	-2.3
ds2	0.726	-0.5	0.611	-1.9	0.561	-2.2
ds3	0.701	-0.4	0.585	-1.3	0.537	-2.9
ds4	0.717	-0.4	0.601	-1.5	0.555	-2.3
ds5	0.735	-0.4	0.605	-1.3	0.559	-2.7
ds6	0.754	-0.4	0.646	-1.4	0.593	-2.2
ds7	0.728	-0.5	0.614	-1.8	0.551	-2.7
ds8	0.754	-0.4	0.649	-1.3	0.594	-2.4
ds9	0.754	-0.5	0.631	-1.5	0.561	-2.0
ds10	0.741	-0.4	0.614	-1.5	0.557	-2.3
ds11	0.751	-0.4	0.640	-1.5	0.599	-2.5
ds12	0.764	-0.4	0.656	-1.3	0.602	-1.5
Average =	0.738	-0.4	0.623	-1.5	0.571	-2.3
σ^2 =	0.02	0.05	0.02	0.204	0.02	0.36
CoV (%) =	2.5	-10.6	3.5	-13.6	3.8	-15.6

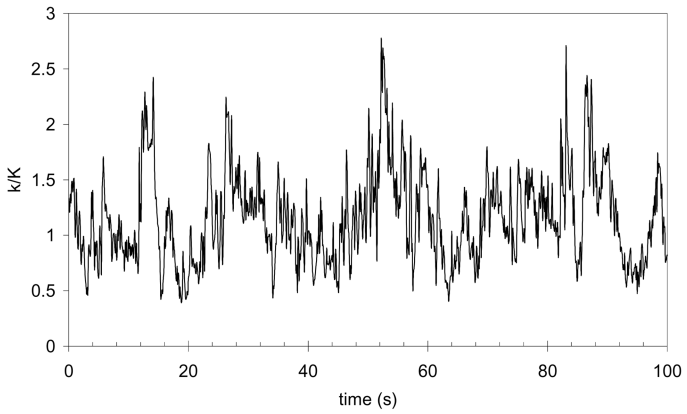

Fig. 6 A snapshot of the instantaneous distribution of kinetic energy

3. Analysis of extreme gusts

3.1. Conditional sampling

Fig. 6 is a snapshot of the instantaneous distribution of the turbulent kinetic energy per unit mass (k) for ds1 where k is defined as, $k = 0.5(u'^2 + v'^2 + w'^2)$. The data in Fig. 6 has been normalised by the average value across the entire dataset (K). Fig. 6 provides striking evidence of the intermittent nature

of the kinetic energy with instantaneous peak values of the order of 3.0 to 3.5 times greater than the average. Associated with these peaks are corresponding low values of k/K illustrating the time varying nature of this variable and suggesting that the spectral analysis undertaken above effectively hides a number of interesting features by averaging them across the entire sampling period. In this section we consider the peak values of this ratio, through the technique of conditional sampling. Extreme/Peak events were defined as when the kinetic energy exceeded the 99.95th percentile value. "Events" less than two seconds apart were taken to be one event with the peak value being given by the greater peak. This resulted in a number of mini time series (see Table 3) which were ensemble averaged. The results of this procedure are shown graphically in Fig. 7 for ultrasonic anemometer 1 ($z = 1$ m) for all

Table 3 Number of peak events identified using different anemometers as a trigger

Dataset	Ultrasonic anemometer 1	Ultrasonic anemometer 3	Ultrasonic anemometer 6	Ultrasonic anemometer 10
ds1	38	31	29	27
ds2	39	25	24	23
ds3	42	30	31	26
ds4	32	30	32	37
ds5	50	38	36	30
ds6	31	26	32	33
ds7	50	41	35	38
ds8	30	19	23	28
ds9	33	28	28	33
ds10	45	36	34	30
ds11	31	20	20	21
ds12	25	24	25	23
Average	37	29	29	29

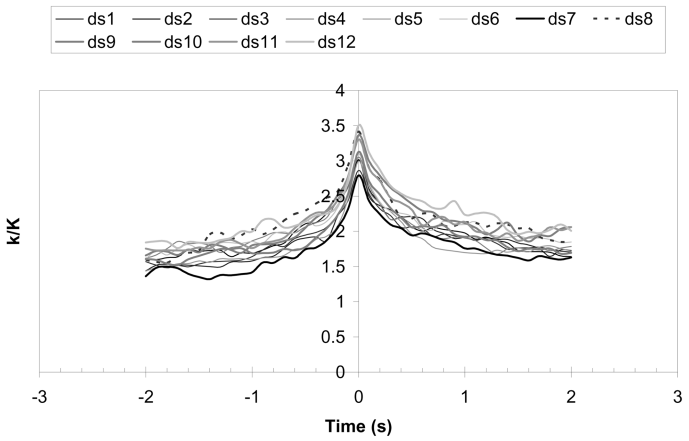

Fig. 7 Ensemble average of the conditional analysis of the normalised kinetic energy, using an extreme event on ultrasonic anemometer 1 as a trigger

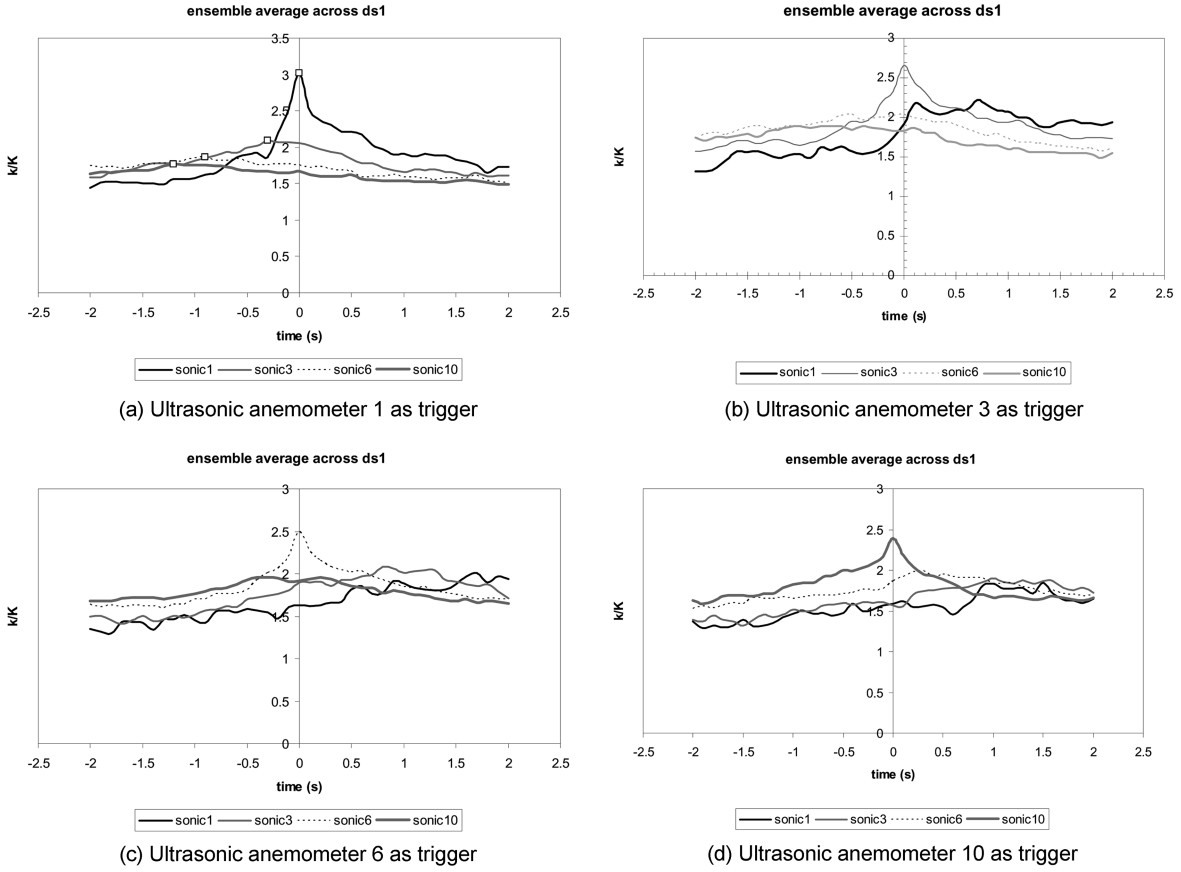

(a) Ultrasonic anemometer 1 as trigger

(b) Ultrasonic anemometer 3 as trigger

(c) Ultrasonic anemometer 6 as trigger

(d) Ultrasonic anemometer 10 as trigger

Fig. 8 Conditional sampling of extreme values – ds1

the datasets. This data illustrates the trends identified by Baker (2001) and Sterling, *et al.* (2003, 2005), i.e., the extreme event is characterised by a short (1 second) peak with a value of the turbulent kinetic energy ratio of around 2.0 superimposed on a much longer term but lower peak with a value of the ratio of around 1.5. It is perhaps also worth noting the apparent lack of symmetry in the gust structure of Fig. 7, i.e., the decrease in normalised kinetic energy occurs at a slower rate immediately after the event than the corresponding increase prior to the event.

Fig. 8 illustrates the effect of using a different ultrasonic anemometer to detect the event. Fig. 8(a) shows the ensemble average for ds1 for an extreme event at ultrasonic anemometer 1 and also illustrates the corresponding trends obtained from the ensemble average of the time series for the remaining anemometers corresponding to the event times identified from the conditional sampling of ultrasonic anemometer 1. In Fig. 8(a) the solid white squares represent the maximum value of k/K and occurs at ensemble times of 0s (ultrasonic anemometer 1, ($z = 1$ m)), –0.2s (ultrasonic anemometer 3, ($z = 3$ m)), –0.6s (ultrasonic anemometer 6, ($z = 6$ m)) and –1.2s (ultrasonic anemometer 10, ($z = 10$ m)). The maximum values of each ensemble time series shown in Fig. 8(a) suggest that on average some flow structure passes through ultrasonic anemometer 10 first, followed by ultrasonic anemometer 6, ultrasonic anemometer 3 and ultrasonic anemometer 1 i.e., this structure is at some angle to the flow. This behaviour is supported by the cross correlation analysis discussed

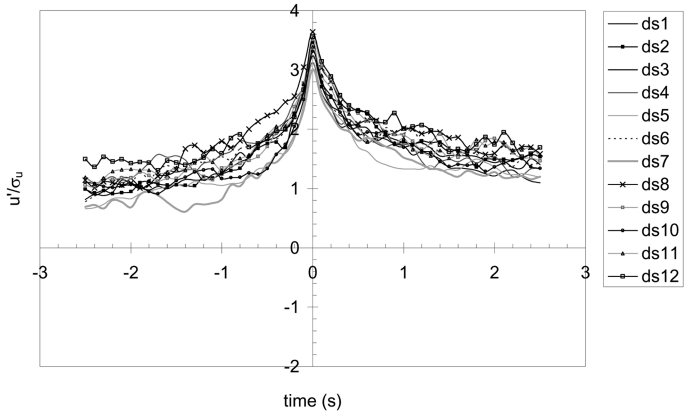

(a) streamwise velocity component

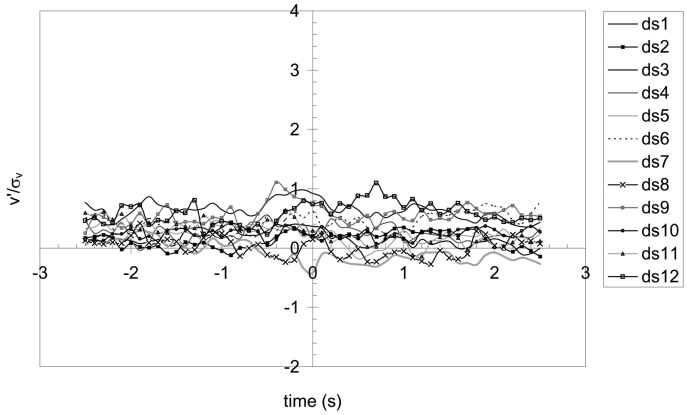

(b) lateral velocity component

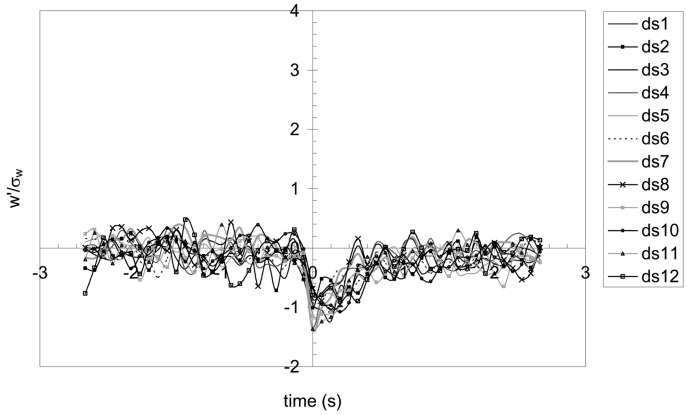

(c) vertical velocity component

Fig. 9 Conditional sampling of the velocity components for ultrasonic anemometer 1, corresponding to the extreme kinetic energy events

above and illustrated in Table 2 and Fig. 5. Using the average cross correlation values shown in Table 2, it is possible to calculate the average angle of inclination of this structure for the current dataset to be 60 degrees to the horizontal by assuming a convection velocity of 0.7 times the local mean velocity. The value of 0.7U is adopted since Adrian, *et al.* (2000) have illustrated that convection velocities of the order of 0.6~0.8 times the mean flow velocity are not unreasonable.

Figs. 8(b), 8(c) and 8(d) illustrate similar results to those shown in Fig. 8(a) but use extreme events at ultrasonic anemometers three, six and ten respectively as a trigger for the conditional sampling. In general it can be seen that the sharp peaks only extend a few metres in height – for example in Fig. 8(d) the peak at ultrasonic anemometer 10 (the trigger) is matched by a slightly later peak at ultrasonic anemometer 6, but no discernable short term peak at the lower ultrasonic anemometers. However for all the anemometers the kinetic energy remains well above its mean value. These results suggest again that there is a large flow structure (with a typical time scale > 8 seconds, with small intense flow structures superimposed upon them. Fig. 8 again highlights that these events are detected at large values of height above the ground first.

Using the event times corresponding to the extremes of turbulent kinetic energy, it is possible to examine the conditionally sampled behaviour of the velocity components at the same time. The results of this relating to ultrasonic anemometer 1 are shown in Fig. 9. In Fig. 9, the vertical axis represents the fluctuating velocity component normalised by its standard deviation. Fig. 9(a) relates to the streamwise velocity component and illustrates similar trends to that of Fig. 8, namely a sharp localised peak either side of the event time. The size of the peak indicates that the streamwise data contributes significantly more than the other velocity components to the instantaneous values of kinetic energy. Fig. 9(b) illustrates the behaviour of the lateral velocity component. It is evident that the distribution of this component is relatively uniform across the entire event time. There is also a rather large variation between each of the datasets, but no other distinctive trends are apparent. Fig. 9(c) relates to the vertical component and possibly illustrates the most interesting behaviour. Prior to the event time ($t = -2.5 \sim -0.1$s) the distributions across all of the datasets are reasonably uniform. However, between $t = -0.1$s and $t = 0$s, a rapid decrease in w'/σ_w is shown in all of the datasets. This suggests that the extreme events are associated with a sweeping motion, i.e., they are directed towards the ground. From $t = 0$s to $t = 1.0$s the velocity gradually returns to a uniform trend similar to that which occurred prior to the event ($t - 0.1$s). This analysis is consistent with that of Richards, *et al.* (2003) who also illustrated there was a discernable negative peak in the vertical velocity data at all heights located with the trigger time, i.e., unlike the streamwise velocity shown in Fig. 8 no delays were noted. This further supports the statement that the peak events are associated with a sweeping motion directed vertically downwards and also suggests that the angle of inclination is rather steep.

Table 3 shows that the total number of extreme events identified at a particular anemometer decreases as the height above ground increases from 1 m to 3 m, but above this height the number of identified events remain constant. However Fig. 10 suggests that some of the events detected at one anemometer are also apparent at other anemometers. A cursory glance suggests that the events appear to be grouped together. In order to investigate if this grouping could have occurred randomly the events from a particular anemometer (e.g. sonic 1, 3, 6 or 10) for all of the datasets were combined, since the actual division of datasets was undertaken for ease of computation. For the case of anemometer one this represented a total of 446 events distributed throughout a twelve hour recording period. The numbers of events occurring within a particular time period, ΔT say, were obtained, from which the probability of occurrence related to that

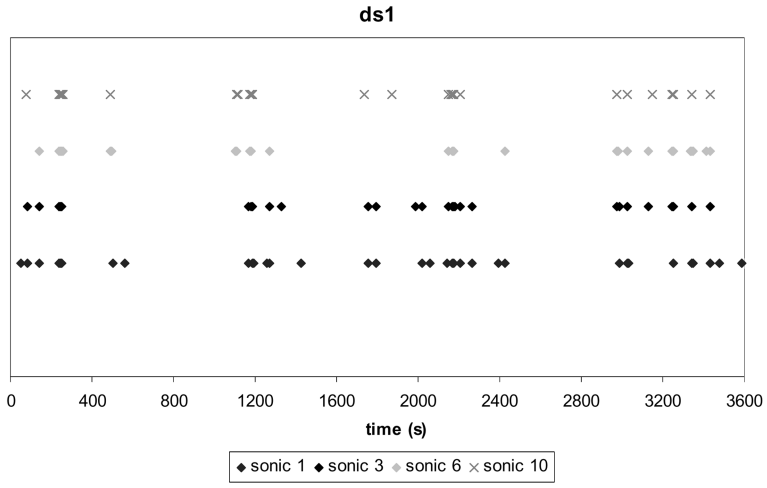

Fig. 10 The distribution of events in the time domain for dataset 1

particular ΔT was established. This probability was then compared to the probability of the same number of events occurring assuming a Poisson distribution (mean = $446\Delta T/(12 \times 3600)$), i.e., assuming the results were random. A χ^2 test was then undertaken to establish the probability that the both the distributions (i.e., the actual obtained from counting the events and the Poisson distributions) were related. This process was repeated for a variety of ΔT values (10s, 50s, 100s, 150s…450s) for all of the anemometers. In all cases the maximum probability that both distributions were related was of the order of 10^{-8}, and in most cases was significantly less than this. Hence it is not unreasonable to conclude that the events which occurred in the current datasets are not randomly distributed in the time domain. A possible reason for this is that the extreme events all occur when the long period flow structure mentioned above has a relatively high velocity, and the peaks are associated with the occurrence of the smaller scale flow structure. The period of the larger scale structure would therefore seem, from a visual inspection of Fig. 10, to be of the order of 400 to 1000 seconds. Assuming that this is convected at a rate of 10 m/s (see Table 1), this gives the size of such structures to be around 4 to 10 km i.e., at the scale of the atmospheric boundary layer.

In order to investigate the simultaneous occurrence of the events further a comparison of the event times obtained when each anemometer was used as a trigger was undertaken. If the difference in event times across all of the anemometers is less than or equal to a specified value then the event is assumed to have occurred across all of the datasets. Table 4 illustrates the results of this process using different values of the time difference. It can be seen from Table 4 that even with the time lag less than 0.5 seconds, six of the datasets show that a number of events have occurred and are registered by all of the anemometers. As the time lag increases from 0.5 seconds or less to 2 seconds or less, the number of large scale events registered expressed as an average across the entire data set, increases significantly from 1.4% to 22.7%. Thus there is an indication that a significant proportion of the extreme energy events, but by no means all, occur more or less simultaneously over some or all of the anemometers, which again suggests that the scale of the short period events identified in the conditional sampling is around 5 to 10 m in height.

Table 4 Percentage of peak events detected across all of the anemometers for various lag/lead times

	Time lag/lead			
Dataset	<= 0.5 secs	<= 1.0 secs	<=1.5 secs	<= 2.0 secs
ds1	2.6%	12.9%	20.7%	22.2%
ds2	2.6%	4.0%	16.7%	21.7%
ds3	2.4%	10.0%	12.9%	27.0%
ds4	3.1%	16.7%	25.0%	24.3%
ds5	0.0%	7.9%	11.1%	20.0%
ds6	3.2%	9.7%	9.7%	22.6%
ds7	4.0%	4.9%	9.4%	18.4%
ds8	0.0%	15.8%	21.7%	21.4%
ds9	0.0%	24.2%	24.2%	39.4%
ds10	2.2%	5.6%	11.8%	23.3%
ds11	0.0%	25%	25.0%	28.6%
ds12	0.0%	8.3%	20.0%	65.5%

3.2. Wavelet analysis

The intermittent nature of the kinetic energy identified in Fig. 6 and the statistical analysis presented earlier has demonstrated the spatial and temporal variability inherent in the wind. This variability probably arises as a result of energy contained within the wind being organized into distinct coherent structures, as evident by the conditional sampling of Section 3. In addition to the techniques employed above it is possible to examine this phenomena using wavelet mathematics. The development of wavelet analysis has now reached a stage where it is possible to analyse the temporal variation of energy with frequency within a given signal. A good description of the use of wavelet analysis is given in Torrence and Compo (1998), and its application to wind engineering are discussed in Gurely and Kareem (1999). In the analysis that follows, the Morlet wavelet has been adopted:

$$\psi(\eta) = \pi^{-1/4} e^{i\omega_o \eta} e^{-\eta^2/2} \tag{2}$$

where η is a non-dimensional time period, ω_o is a non-dimensional frequency, here taken to be 6 (Farge 1992) and $i = \sqrt{-1}$. Twenty-one distinct scales or periods were used in the analysis and ranged from 0.2 seconds to 204.8 seconds. These scales were based on powers of 2 in order to provide information across the appropriate range of the frequency spectrum. For each time series this resulted in a set of 21 time series of the same length across the range of periods. In order to provide a detailed analysis regarding the extreme events identified earlier, the event times identified in Section 3.1 where used to obtain an ensemble average of the normalised wavelet power at each scale. The results of this process are shown in Fig. 11(a) for ds1, ultrasonic anemometer 1. In Fig. 11(a) the instantaneous value of wavelet power has been normalised by the average power at the corresponding scale. The same analysis has been undertaken for all of the data series and follows similar trends to those reported, however for the purposes of brevity attention is restricted to ds1. A large localised peak at the event time ($t = 0$) is noticeable for the smallest scale (highest frequency =

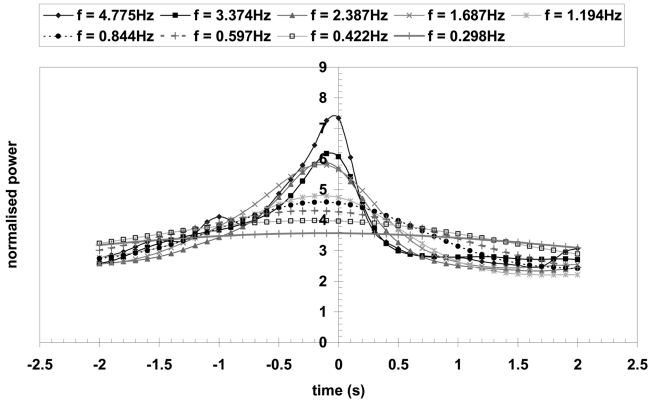

(a) Mini ensemble average time series of wavelet power identified using conditional sampling. Scales 1-6, ultrasonic anemometer 1

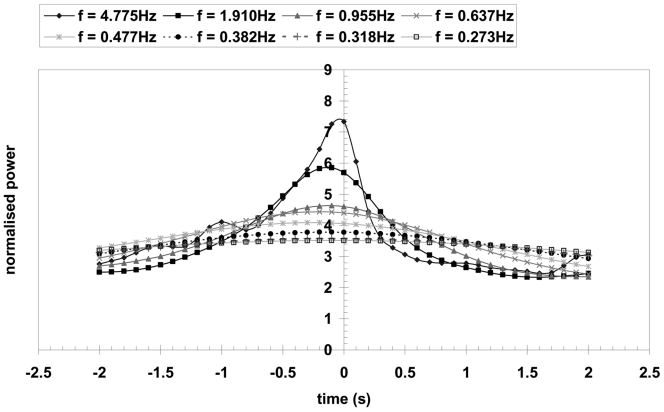

(b) An ensemble average across the entire data sets using the revised wavelet scales, ultrasonic anemometer 1

Fig. 11 Wavelet analysis

4.775 Hz) sampled. This behaviour is also shown, albeit to a lesser extent for frequencies above 1 Hz. Below these frequencies there is a less of a noticeable peak around the event time, however the normalised power is greater than or equal to two across the entire sampling period. This again suggests the presence of a small localised event superimposed on a structure of larger scale and further shows a transfer of energy from lower frequencies towards higher frequencies around the peak. The sampling period of 4 seconds essentially introduces a filter corresponding to 0.25 Hz, which is why no data with a frequency below 0.25 Hz is illustrated.

In order to examine the high frequency behaviour in more detail, a further wavelet analysis was undertaken but this time the scale chosen were restricted i.e., the base of the scales were not raised to the power of 2. Using the times corresponding to the events of Table 3, a conditional analysis of the normalised kinetic energy of the wavelet time series corresponding to the scales of Table 5 was undertaken. This produced an additional 3568 mini time series (446 times × 8 different scales). For each scale, these 446 mini time series were ensemble averaged in order to provide an insight into the behaviour of the flow structures and the results of this process are shown in Fig. 11(b).

Table 5 Revised wavelet scales used to investigate the ensemble average of k/K

	1	2	3	4	5	6	7	8
Scale	0.2	0.5	1.0	1.5	2.0	2.5	3.0	3.5
n	4.775	1.910	0.955	0.637	0.477	0.382	0.318	0.273

Fig. 11(b) supports the findings presented earlier, namely that a significant amount of energy exists at high frequencies ($n = 4.775$ Hz) and is located at the event time. What is apparent from Fig. 11(b) is that for all frequencies the value of normalised power across the sampling period remains relatively large supporting the findings presented earlier, i.e., at the extreme events there are two distinct flow mechanisms of different scales occurring at the same time. The results Fig. 11 support the conditional sampling of the normalised kinetic energy presented earlier (Fig. 7) in that it is apparent that the increase in k/K value close to the event time ($t = 0$) can be related to the high frequency wavelet components shown in Figs. 12 and 13.

4. Turbulence structures in the atmospheric boundary layer at extreme events

From the work of the last section it would appear that two distinct turbulence structures are found when extreme events occur in the atmospheric boundary layer. The first of these is a large low frequency structure that appears to have a scale of the order of the atmospheric boundary layer thickness, with length scales of around 4 km, and time scales of the order of tens of minutes. The second is a much smaller scale structure that seems to have a time scale of around 1 second and a length scale (in terms of both height and length) of around 10 m. These structures are inclined at an angle to the flow of around 60 degrees in the situation discussed here. This inclination is consistent with the cross spectral analysis of data from the same site of Richards, *et al.* (2003) who used the same data albeit for a different purpose to that in this paper. The work of Sterling, *et al.* (2005) suggests that these small structures are regions of high vorticity, with both significant velocity and pressure changes. Extreme events occur when the velocity within these two types of structure have maximum values at a particular point i.e., during the peak velocity period of the large scale structure (which last for 10 to 100 seconds), the passage of a small scale structure will result in the extreme velocities being measured.

Of course the situation is not as deterministic as the above description would suggest. One can assume that the large scale structures correspond to the lower end of the velocity power spectra shown in Fig. 3, whilst the small scale structures correspond to the higher end of the frequency range. There is a continuous energy spectrum between them due to the energy dissipation process that occurs in any turbulent flow. However it does seem that, *at extreme events*, it is possible that on average these two types of structure can be distinguished.

This discussion of course leaves many unanswered questions – for example the question arises as to how these flow structures may vary with parameters such as surface roughness length, Reynolds number etc. Also it is perhaps worth noting that for the small scale structures, a time scale of 1s is approximately equivalent to a length scale of 10 m, at an average velocity of 10 m/s.

There are also significant implications for this work in terms of studies of extreme wind loading. It is possible to conceive of a model of extreme wind conditions that is based on the superposition of the two turbulence structures described in this paper – a low frequency, predominantly quasi-steady component, that scale on atmospheric boundary layer size, and a high frequency inclined

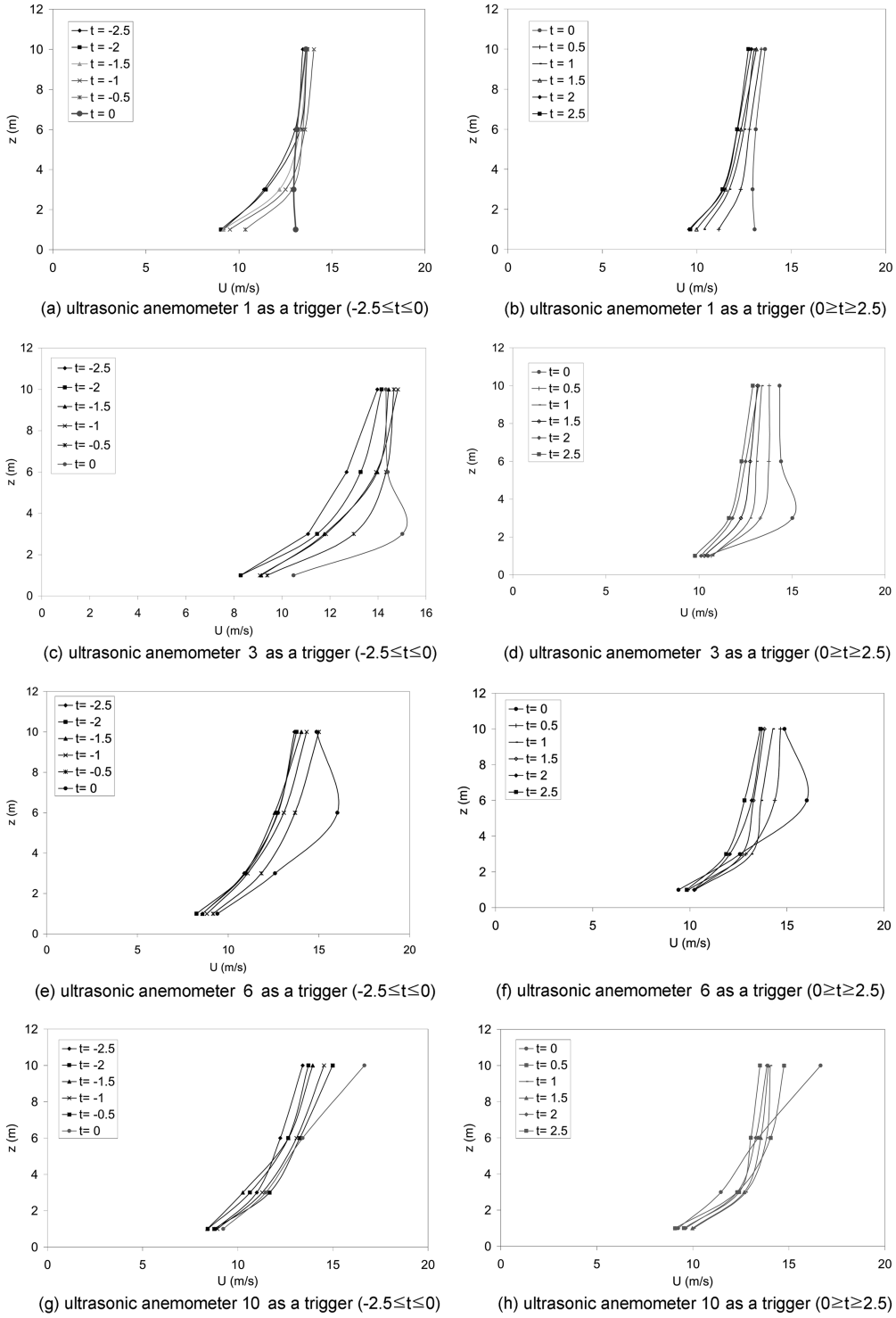

(a) ultrasonic anemometer 1 as a trigger (-2.5≤t≤0)

(b) ultrasonic anemometer 1 as a trigger (0≥t≥2.5)

(c) ultrasonic anemometer 3 as a trigger (-2.5≤t≤0)

(d) ultrasonic anemometer 3 as a trigger (0≥t≥2.5)

(e) ultrasonic anemometer 6 as a trigger (-2.5≤t≤0)

(f) ultrasonic anemometer 6 as a trigger (0≥t≥2.5)

(g) ultrasonic anemometer 10 as a trigger (-2.5≤t≤0)

(h) ultrasonic anemometer 10 as a trigger (0≥t≥2.5)

Fig. 12 Distribution of streamwise velocity distribution throughout an event using various ultrasonic anemometers to detect the events (ds1)

vortex component. The extreme loads on the structure would be caused by a combination of a global quasi-steady effect due to the large scale structures and a load due to the distortion of vorticity around the structures. The latter component could potentially interact strongly with body induced vorticity such as found in separated shear layers, roof corner vortices etc.

With respect to structural loading the distribution of streamwise velocity with height above the ground is of practical importance, particularly at the onset of the extreme events discussed above. Using the data illustrated in Fig. 9(a) it is possible to calculate the average velocity profile across all of the data sets for various times relating to the extreme events. This behaviour is illustrated in Fig. 12. Figs. 12(a) and 12(b) illustrate the evolution of the streamwise velocity profile throughout the extreme event time when events detected at ultrasonic anemometer 1 are used as a trigger. It is evident that for this particular case the event engulfs the whole array of ultrasonic anemometer anemometry and results in a uniform velocity profile. Figs. 12(c) – 12(h) investigates the evolution of the velocity profile using extreme events detected at the remaining ultrasonic

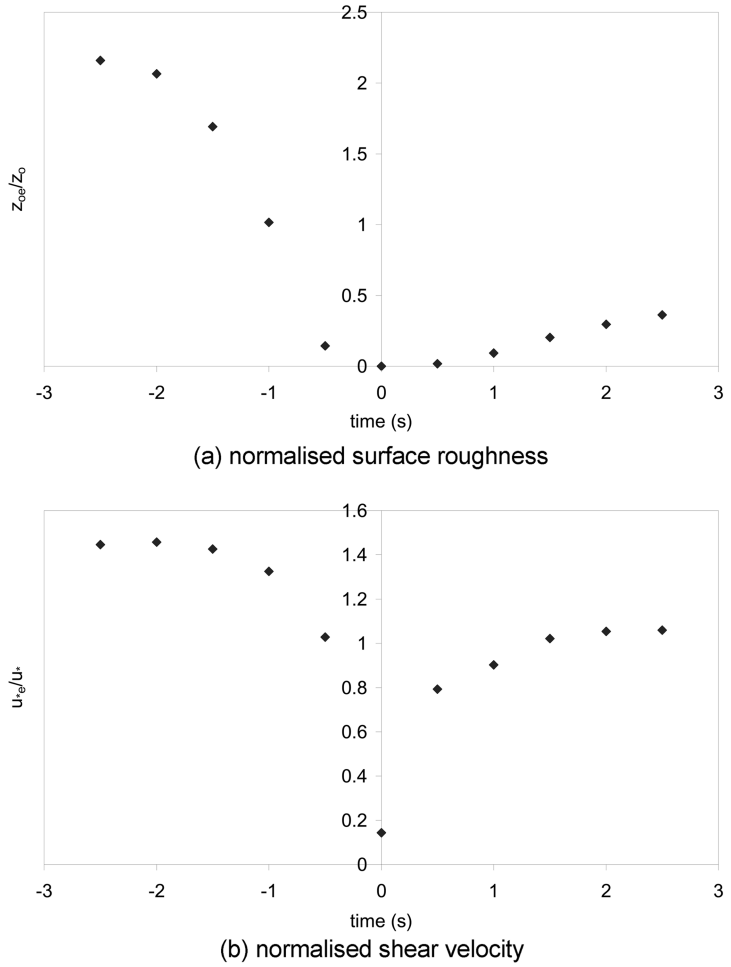

Fig. 13 Changes in instantaneous normalised surface roughness and shear velocity during an event for events detected at ultrasonic anemometer 1 (ds1)

anemometers. When ultrasonic anemometer 3 is used as the trigger it is evident that on average the local velocity at all heights increases, but the velocity profile at the occurrence of the event ($t = 0$) is not as uniform at that shown in Fig. 12(b). Similar behaviour is illustrated in the data pertaining to other the anemometry, and suggests that on average the location of the large scale structure does not engulf the array of ultrasonic anemometers. This may simply be due to the location of the anemometry with respect to the large flow scale structure as it impacts on the ground. Immediately before and after the event, the velocity profiles appear to follow a logarithmic distribution. Figs. 13(a) and 13(b) illustrate the normalised surface roughness (z_{oe}/z_o) and shear velocity (u_{*e}/u_*) evolution during the event. The values of z_{oe} and u_{*e} are obtained by fitting a logarithmic law to the instantaneous velocity profile, however as it will be discussed later this is not necessarily a sensible approach. The normalisation parameters represent the nominal values of surface roughness and shear velocity given in Table 1. The decrease in surface roughness when ultrasonic anemometer 1 is used as a trigger is noticeable in Fig. 13(a). It is also evident that from this figure that once the event occurs, the velocity profile slowly tends towards equilibrium, i.e., there is a rapid shift prior to the event but a more gradual change after the event. This behaviour is also supported by the results illustrated in Figs. 7 and 9(a). At the event time, there is a rapid decrease in friction velocity suggesting a possible local minimum in shear stress. However, this is an incorrect interpretation as shown by the results in Figs. 9(a) and 9(c), i.e., the Reynolds stresses attain a maximum value. The local minimum in shear velocity simply reflects the inadequacy of the log law to represent the velocity distribution during extreme events.

In the above analysis attention has been restricted to events 2.5s either side of the peak. However, it may be of interest, particularly if such phenomena are to be modelled correctly to gain an indication of the extent to which these low frequency, large scale components extend. In order to investigate this behaviour a conditional analysis identical to that outlined in Section 3 was undertaken on the streamwise velocity component with the exception that the event time was extended to 30s either side of the peak. The 60s time window was chosen based on a number of successive trials and appears to offer the best compromise between analysing the low frequency behaviour while at the same time preserving the data on the high frequency behaviour associated with the peak events. In other words the larger the time window the greater the possibility of identifying a number of events above the desired threshold value which will ultimately be lost in the analysis since only the greatest value of velocity within the time window are assumed to be the peak event. The streamwise velocity component was chosen since for this analysis rather than the kinetic energy since it was considered that information regarding this parameter would be of greater interest to those involved in wind loading studies. Fig. 14(a) illustrates the ensemble average of the normalised streamwise velocity for all of the events extending across the entire dataset at a particular anemometer when the same anemometer is used as a trigger. From Fig. 14(a) it is noticeable that all of the four curves appear to indicate almost identical behaviour. Hence, it is perhaps not unreasonable to postulate that the shape of the event is independent of the trigger position and if this is the case then it is permissible to combine all of the event time series obtained across all of the datasets at different heights to form an ensemble average. The results of this analysis are shown in Fig. 14(b). Also shown in Fig. 14(b) is a simple curve of the form:

$$\frac{u}{U} = B\left[\frac{|t|}{b} + 1\right]^m \tag{3}$$

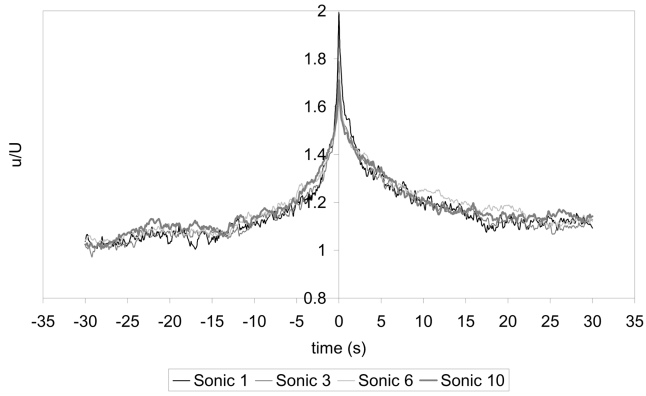

(a) Ensemble average of normalised streamwise velocity all datasets

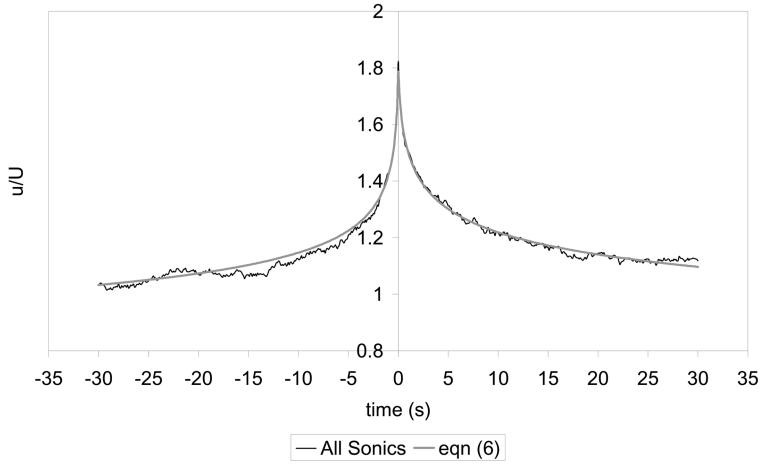

(b) Ensemble average of normalised streamwise

Fig. 14 Velocity across all datasets across all anemometers

where:

time	B	b (s)	m
$-30 \le t \le 0$	1.786	0.10	-0.096
$0 \ge t \ge 30$	1.786	0.20	-0.097

This curve has been fitted to give an indication of the overall shape of the event distribution with respect to time. It does not have any physical basis nor do the authors suggest it is the best possible fit. Eq. (3) merely appears to illustrate the trend reasonably well, ($R^2 \sim 98\%$). Alternatively, a similar expression for $(u - U)/U$ can be obtained with the added benefit that that as $t \rightarrow \pm\infty (u - U)/U$ tends towards zero. However, this approach has not been adopted since Eq. (3) allows the estimation of the time scale of the peak event, i.e., when $u/U = 1.0$, which using the above values is calculated to be of the order of 120s. Assuming that this structure is convected with a mean velocity of 10 m/s the corresponding scale is 1.2 km which is consistent with the scales estimated from Fig. 10.

5. Conclusions

From the work of the preceding sections the following conclusions can be drawn.

(a) The flow over a rural terrain with an unobstructed fetch has been analysed using conventional and non conventional methods. Although relatively stationary, the flow has been shown to be highly complicated. Nonetheless the statistical moments, autocorrelations and spectra show that the boundary layer has all the characteristics that would be expected of a well developed rural boundary layer.

(b) The instantaneous kinetic energy has been shown to be highly intermittent in nature and conditional sampling appears to indicate that the extreme gusts are associated with a small scale flow structure (of about 1 to 2 seconds duration) superimposed on a large scale flow structure of around 100 seconds duration. The small scale structures seem to have a vertical scale of around 10 m. The results confirm the findings of earlier work (Sterling, *et al.* 2003, Baker 2001) namely that small scale, high frequency vortex structures are present in the flow and contain a significant amount of energy.

(c) Wavelet analysis has been successfully combined with the conditional sampling and has provided an insight into the distribution of energy with frequency during extreme events.

(d) During an extreme event, when ultrasonic anemometer 1 is used as a trigger the streamwise velocity profile has been shown to tend towards a uniform distribution with height.

Acknowledgements

The first author is grateful to the Nuffield foundation whose generosity through the Newly Appointed Lectures Awards programme (NUF-NAL/00674/G) made the data analysis possible.

References

Adrian, R.J., Meinhart, C.D. and Tomkins, C.D. (2000), "Vortex organisation in the outer region of the turbulent boundary layer", *J. Fluid Mech*., **422**, 1-54.

Baker, C.J. (2001), "Unsteady wind loading on a wall", *Wind and Struct., An Int. J.*, **4**(5), 413-440.

Baker, C.J. (2005), "Wind engineering - past, present and future", Key Note Address. *4th European & African Conference on Wind Engineering*, Prague. 11-15 July.

ESDU (1985), "Characteristics of atmospheric turbulence near the ground: Part 2 single point data for strong wind - neutral atmosphere", data Item 85020, Engineering Sciences Data Unit, London.

Fiedler, H.E. (1988), "Coherent structures in turbulent flows", *Progress in Aerospace Sciences*, **25**, 3, 231-269.

Garde, R.J. (1994), *Turbulent Flow*, Wiley Eastern, New Delhi.

Gurley, K. and Kareem, A. (1999), "Application of wavelet transforms in earthquake, wind and ocean engineering", *Eng. Struct.*, **21**, 149-167.

Jeong, J. and Hussain, A.K.M.F. (1995), "On the identification of a vortex", *J. Fluid Mech.*, **285**, 69-94.

Kaimal, J.C. and Finnigan, J.J. (1994), *Atmospheric Boundary Layer Flows*, Oxford University Press, U.K.

Richards, P.J., Fong, S. and Hoxey, R.P. (1997), "Anisotropic turbulence in the atmospheric surface layer", *J. Wind Eng. Ind. Aerodyn.*, **69-71**, 903-913.

Richards, P.J., Baker, C.J. and Hoxey, R.P. (2003), "Turbulent event sequencing in the atmospheric surface layer", *11th International Conference on Wind Engineering*, Lubbock, Texas, 2-5 June 2003, 2101-2108.

Richards, P.J., Hoxey, R.P., Connell, B.D. and Lander, D.P. (2005), "Wind tunnel modelling of the Silsoe Cube", *The fourth European & African Conference on Wind Engineering*, July 11-15, Prague.

Robertson, A., Hoxey, R.P., Quinn, A.D., Hobson, N. and Burgess, L. (2001), "The atmospheric flow laboratory ay silsoe research institute: A new facility for wind engineering", *3rd European & African Conference on Wind*

Engineering, Eindhoven University of Technology, 2-6 July 2001.
Sterling, M., Baker, C.J. and Hoxey, R.P. (2003), "Short term unsteady wind loading on a low-rise building", *Wind and Struct., An Int. J.*, **6**(5), 403-418.
Sterling, M., Baker, C.J., Quinn, A.D. and Hoxey, R.P. (2005), "Pressure and velocity fluctuations in the atmospheric boundary layer", *Wind and Struct., An Int. J.*, **8**(1), 13-34.
Stull, R.B. (1988), *An Introduction to Boundary Layer Meteorology*, Kluwer Academic Publishers, 684 pages.
Torrence, C. and Compo, G.P. (1998), "A practical guide to wavelet analysis", *Bulletin of American Meteorological Society,* **79**(1), 61-78.

Notation

B	constant in Eq. (3)
b	constant in Eq. (3)
CoV	coefficient of variation = mean/standard deviation
f	dimensionless frequency = nz/U
I_i	turbulence intensity corresponding the the ith component of velocity
k	instantaneous turbulent kinetic energy (m^2/s^2)
K	mean turbulent kinetic energy (m^2/s^2)
L	characteristic length
L_{mo}	Monin-Obukhov length (m)
m	exponent in Eq. (3)
n	frequency (Hz)
$S_i(n)$	velocity spectra corresponding to the ith velocity component
u'	instantaneous streamwise velocity (m/s)
U	mean streamwise velocity (m/s)
u_*	friction velocity (m/s)
u_{*e}	Instantaneous value of friction velocity during a peak event (m/s)
v'	instantaneous lateral velocity (m/s)
V	characteristic velocity
w'	instantaneous vertical velocity (m/s)
x	streamwise direction (m)
${}^xL_u$	Streamwise length scale in corresponding to the u component (m)
y	lateral direction (m)
z	vertical direction/height above the ground (m)
z_o	Mean value of surface roughness (m)
z_{oe}	Instantaneous value of surface roughness during a peak event (m)
κ	von Karman constant
ω_o	non-dimensional frequency time period relating to wavelet analysis
θ	potential temperature